Available online at www.sciencedirect.com
SCIENCE DIRECT®
Journal of Magnetism and Magnetic Materials 272–276 (2004) 1130–1134
Journal of magnetism and magnetic materials
www.elsevier.com/locate/jmmm

The magnetism of ultrathin trilayers: a playground to study fundamentals

Klaus Baberschke*

Institut für Experimentalphysik, Freie Universität Berlin, Arnimallee 14, D-14195 Berlin-Dahlem, Germany

Abstract

Pseudomorphic growth of ultrathin magnetic trilayers offers unique possibilities to study magnetic phenomena, e.g. the magnetic anisotropy energy and interlayer exchange coupling can be enlarged by orders of magnitude, the Curie temperature can be varied from zero to T_C^{bulk}, effects of spin fluctuations in 2D become observable, etc. We prepare, modify step by step, and measure the films in situ by applying various experimental techniques (FMR, XMCD, etc.) in UHV. The results compare very well with theory and ab initio calculations.

PACS: 75.70.−i; 76.50.+g; 78.70.Dm

Keywords: 2D films; Curie temperature; Spin fluctuations; Review

1. Introduction

Two ferromagnetic films, separated by a nonmagnetic spacer, all three of a few atomic layers thickness only, represent the archetype of magnetic multilayers and nanostructures. These 'trilayers' offer a full variety of external parameters to manipulate its magnetism [1–4]. Prominent features, which are not accessible in bulk magnetism, are:

(i) Special growth and film preparation methods allow to prepare crystallographic structures, like tetragonal Ni or trigonal Co which cannot be produced for bulk single crystals. These structures can be stable up to 10–20 monolayers (ML), in some cases by surfactant-assisted growth. These small departures from cubic fcc or bcc structures do have significant consequences. The formally quenched orbital magnetic moment μ_L gets reactivated. This in turn enlarges the magnetic anisotropy energy (MAE), i.e. changes of 0.03–0.05 Å may increase the MAE by 10^2–10^3.

(ii) A second 'knob to turn on' is the Curie-temperature T_C. Via the film thickness d and the finite size effect, T_C can be shifted to almost any value between zero and T_C^{bulk}. For example, T_C^{Ni} may be larger than T_C^{Co}. It is important to realize that for many magnetic properties, T_C is a fixpoint. That is to say, since T_C depends on the thickness, it is important to scale the observables as a function of the reduced temperature $t = T/T_C$. The thickness d of a ferromagnetic ultrathin film not only changes T_C, but also controls the dimensional crossover from 3D $\Rightarrow$ 2D.

(iii) The interlayer exchange coupling (IEC), the strength as well as the sign of the coupling can be manipulated via the spacer thickness. We discuss recent ferromagnetic resonance FMR experiments, which allow to measure the ferro- as well as antiferromagnetic coupling, both in absolute energy units (eV/particle) as well as their temperature dependence.

(iv) Another focal point is the importance of the magnetism at the interface itself. Here the use of synchrotron radiation and X-ray magnetic circular dichroism (XMCD) is a very powerful technique: Not only the element specificity allows to measure all moments (including the induced magnetism at nonmagnetic spacers) separately, but also the signal can be decomposed into orbital and spin moments μ_L and μ_S, respectively.

*Corresponding author. Tel.: +49-30-838-52648; fax: +49-30-838-53646.
E-mail address: bab@physik.fu-berlin.de (K. Baberschke).

0304-8853/$ - see front matter © 2004 Published by Elsevier B.V.
doi:10.1016/j.jmmm.2003.12.760

Finally, we mention that this field of research demonstrates very successfully the collaboration between theory and experiment.

2. MAE and IEC in a trilayer: experiment vs. theory

The most informative way to study the electronic and magnetic structure of a trilayer is to build up in situ the trilayer step by step in UHV. In Fig. 1 the bottom trace shows the (0,0) I–V LEED intensity for the substrate Cu(0 0 1) crystal. The various diffraction peaks correspond to a layer spacing of 1.81 Å. For the subsequent pseudomorphically grown 9 ML Ni, 6 ML Cu, and 8 ML Ni, the peaks are shifted to higher energies corresponding to −5.5% contraction of the layer spacing [5,6]. Small uniaxial distortions of few percent do have dramatic effects in the MAE [7,8]. This is obvious because there exist only two principal mechanisms to create anisotropy in the magnetic part of the free energy: (i) the dipole–dipole interaction ($\approx 2\pi M^2$), which depends on the shape of the specimen and is of less interest here, and (ii) the *intrinsic* anisotropy energy K originating from the spin–orbit interaction (SO), or a nonspherical charge distribution, respectively. There exists no other mechanism; crystal field, magneto-elastic effects, etc., they all do have the same origin, namely SO! Consequently, for ab initio calculations, it is important to perform an accurate relativistic calculation of the difference in free energy (full relativistic, or full potential, etc.). This has been recently performed for single layers [9]. In Fig. 2 we show the same type of calculation by the same group [6] for our trilayer in question. The theory calculates the relativistic spin-polarized 'band energy' difference ΔE_B^j, which can be brought in contact with the experimentally determined *intrinsic* MAE, which may be decomposed into a volume and surface (averaged) part, i.e. $K = K_V + 2K_S/d$. We

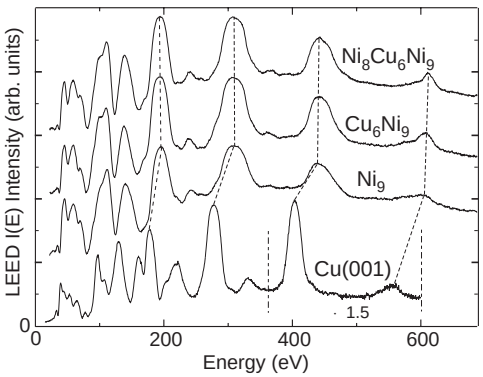

Fig. 1. Intensity vs. energy of the LEED (0,0) beam at normal incidence for the substrate crystal and after successive evaporation of two ferromagnetic Ni films and a Cu spacer.

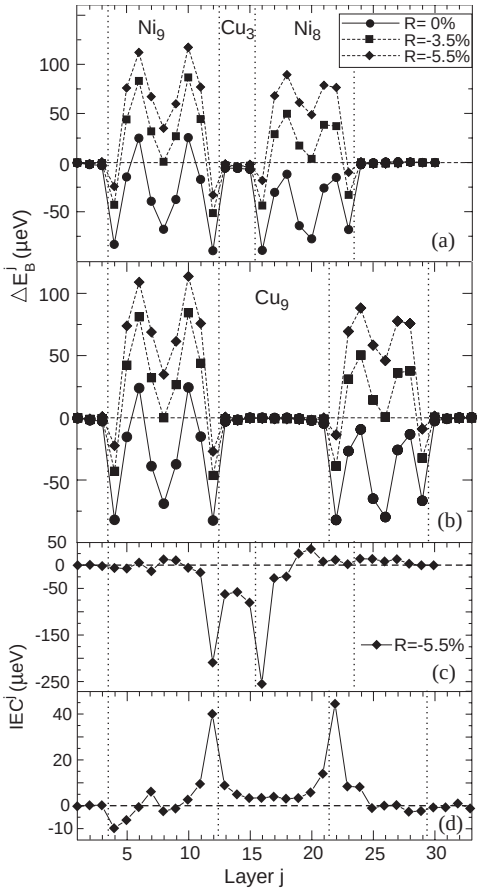

Fig. 2. Layer-resolved band energy difference ΔE_B^j for the trilayer as given in Fig. 1. The Cu spacer was changed to 3 ML (a) and to 9 ML (b), (c) and (d) show the corresponding IEC values.

see clearly in Fig. 2a and b that increasing relaxation from 0% to −5.5% shifts the anisotropy energy to higher positive values. The Ni layers at the interfaces remain negative, but the central part 'K_V' moves to large positive values. *The tetragonal distortion with a relaxation in the layer spacing is the dominant contribution to the MAE—not the surface part*. This also controls the spin reorientation transition. As experimentally evidenced, the fct structure also exists in the top part of the trilayer. We learn from Fig. 2a and b that the Cu_3 and Cu_9 spacer do not contribute to ΔE_B^j, only the Ni layers are important. This is different for the IEC. In Fig. 2c, d we see that the Ni layer at the interface is dominant, but in addition also the Cu layers at the interface contribute to the exchange coupling. For a very thin spacer Cu_3, all three layers are relevant. The experimental K and J_{inter} values are defined from the differences in the free energy and are consequently temperature dependent [10]. In the theory constant values of ΔE_B^j and IEC^j at $T = 0$ exist,

and both are interrelated with K and J_{inter} but not identical.

3. Enhanced spin fluctuations in ultrathin trilayers

Let us take a trilayer with Co on top and Ni at the bottom. Does such a film undergo one phase transition (if exchange coupled) or does Co and Ni show separate T_C's? Can we define more than one order parameter? To address this question experimentally, the most suitable technique is X-ray absorption spectroscopy (XAS); each element can be measured separately at the element-specific X-ray absorption edges. With XMCD we are even sensitive to the magnetization of each element. This problem has been addressed recently, and the results are summarized in Ref. [11]. By reducing the Co thickness to 1–2 ML it was possible to obtain $T_C^{Co} < T_C^{Ni}$ [12]. The problem is shown schematically in Fig. 3. A single 4 ML Ni film capped with Cu orders at $T_C^{Ni} \approx 215$ K. After deposition of 2.8 Co on top, XMCD has two options. First we observe the new Co signal. Clearly, the magnetization is larger (approximately by a factor of three corresponding to the magnetic moments) and also T_C^{Co} is much higher. If we now monitor again the first Ni film (full circles), we see that the magnetization is shifted to much higher values by $\Delta T_C \approx 80$ K. At first glance one would argue that the exchange field of the strong ferromagnet Co acts like an additional static field resulting in a larger field-induced magnetization. However, a simple estimate shows that static fields of several Tesla will shift the magnetization to higher values only by a few K. A shift by 80 K with respect to a T_C of 215 K is completely unexpected and has never been observed in bulk ferromagnets. That is to say, such an effect cannot be explained in terms of a simple mean field picture where only $\langle S_z \rangle$ is taken into consideration. This experimental finding is very evident and proves unambiguously that in ultrathin film magnetism,

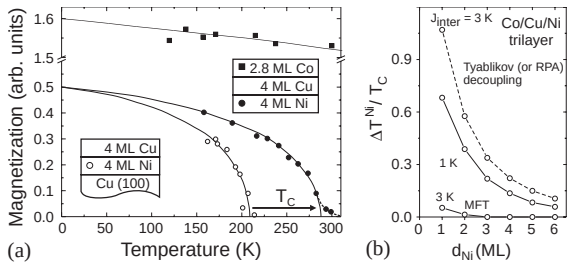

Fig. 3. (a) Temperature dependence of M measured by means of XMCD. Open circles show the single Ni film capped with Cu only. The full symbols correspond to the trilayer. The XMCD was measured in a small external field of 20–40 Oe, to avoid domain formation; (b) Theoretical calculated shift of ΔT^{Ni} in mean field (MFT) and RPA approximation as a function of the Ni thickness d_{Ni} [13].

higher order effects i.e. spin fluctuations $\langle S^2 \rangle$ have to be considered. This has been very nicely proven theoretically by Jensen et al. [13] and is displayed in Fig. 3b. Clearly an MFT ansatz taking a realistic exchange coupling of $J_{\text{inter}} = 3$ K shifts T_C by only 1–2% for a few ML Ni. If one keeps the strength of interlayer exchange coupling constant but calculates the same observable in a higher order approximation (e.g. Tyablikov decoupling) we see that for 2 ML the increase of T_C shifts up to $\approx 60\%$. Furthermore, we can see from Fig. 3b that this higher order effect of spin fluctuations becomes most dramatic the thinner the Ni film. In summary, these element-specific XMCD measurement on a Co/Cu/Ni trilayer is to our knowledge, the most evident proof that spin fluctuations in ultrathin films and at interfaces are much more dramatic than in bulk magnetism—it may also lead to more advanced theoretical calculations of spin injection mechanisms (due to space restrictions here we refer for further discussion on T_C to Ref. [11]).

4. Optic and acoustic spin wave branches, 'Non-Gilbert-like' spin wave damping

Two exchange coupled ferromagnetic films exhibit two eigenmodes of the uniform motion of the magnetizations M_1 and M_2—in analogy to coupled pendula (Fig. 4, top). In analogy to the notion of phonon branches, they are labeled acoustic (in-phase) and optic (π out-of-phase) modes. The FMR is the technique of choice to investigate this spin wave dynamics: FMR measures both AFM and FM coupling, it determines MAE, IEC and all parameters in absolute energy units. Most other techniques (e.g. MOKE) have difficulties to do so. The most important feature of our experiments is the in situ UHV-FMR with a step-by-step measurement. Using the Landau–Lifshitz (LL) equation of motion

$$\frac{1}{\gamma}\dot{\vec{M}} = \vec{M} \times \vec{H} + \frac{G}{\gamma M^2}(\vec{M} \times \dot{\vec{M}}), \tag{1}$$

we simulate the FMR spectra (Fig. 4, middle). For $J_{\text{inter}} = 0$ with no coupling, two resonances with equal intensity are observed. Increasing coupling strength for FM ($J > 0$) and AFM ($J < 0$) coupling shifts the resonance and its intensity for both modes (for details, see Ref. [14]). In the bottom part of Fig. 4 we show the experimental realization of the 'step-by-step' UHV-FMR. Firstly, we prepare and measure a single Co_2 (Ni_9) film capped with Cu (dotted line). Than we evaporate in situ a second Ni_7 (Ni_8) film. The left (right) case shows AFM (FM) coupling. The fit with the LL equation (dashed line) shows perfect agreement, yielding all basic parameters, i.e. M, $K \leftrightarrow \Delta E_B$, and $J_{\text{inter}} \leftrightarrow$ IEC given in μeV/particle [14] and its huge temperature dependence [10].

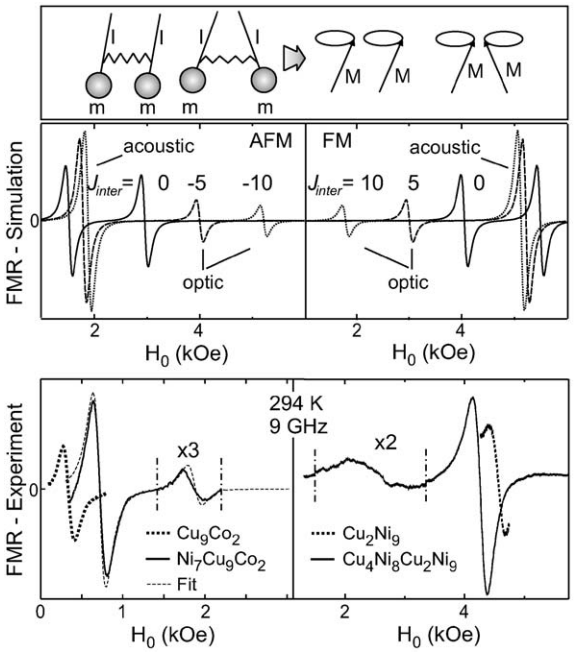

Fig. 4. Top: sketch for coupled pendula and magnetizations; Middle: Simulation of FMR for optical and acoustical modes in a trilayer with AFM and FM coupling. Bottom: corresponding experimental FMR spectra.

The linewidth of the FMR gives information on the spin dynamics, and in addition, the relaxation of M. Commonly, this is taken into account with a Gilbert damping term in the LL equation. This Gilbert damping is mostly used to explain and calculate spin memory effects, spin dynamics for femtosecond pulses, etc. However, this ansatz has severe restrictions: dM/dt implies a damping being proportional to ω. Recently, we have given experimental evidence that a second mechanism, i.e. magnon–magnon scattering, is equally important at interfaces of nanostructures. Details will be published elsewhere [15].

5. Induced orbital and spin moments at interfaces

Interfaces of ferro- and non-magnetic nanostructures are of particular interest, e.g. spin-polarized currents across the interface, spin wave excitations a.o., all will depend on the local geometrical and electronic structure as well as on the induced magnetic moment for the non-magnetic constituent and also on the modified μ_L and μ_S values. In early days 'dead layers' at surfaces and interfaces were postulated; with today's knowledge one might say 'dead layers are dead'. Numerous experiments by various groups did show that small fraction of an ML of residual gas might form oxides (e.g. NiO) and that this layer does not contribute to the saturation magnetization of ferromagnetism and was falsely interpreted as if the magnetic moment per atom was zero. An ideal interface of elements A/B has a perfect ordered local structure, namely 50% nearest neighbor of A and 50% of B. In principle this should be completely different from a 50% alloy, where we have a statistical distribution of nearest neighbor A and B atoms. On the other hand, the breaking of local symmetry will have a dramatic influence, for example, on the lifting of quenching of μ_L and one should not assume a priori that alloy physics and interface effects are the same [16].

XAS and XMCD are the techniques of choice to investigate the electronic and magnetic structure of interfaces in an element-specific way. The technique is not layer sensitive per se, but by varying the number of interface layers one also obtains a layer-sensitive information. This is demonstrated for Ni/Pt multilayers in Ref. [17].

In Fig. 5 a $Fe_5/V_3/Fe$ trilayer is shown schematically. V as a metal is nonmagnetic, but it is known that at the Fe interface V does carry a magnetic moment. First of all we point out the high sensitivity and signal-to-noise ratio for the XMCD spectra of a single 3 ML V film. Such a spectrum can be taken at BESSY II in 20 min free of noise (Fig. 5a). On the right-hand side, the corresponding Fe spectra are plotted and we see immediately that the induced V moment is aligned antiparallel to Fe (opposite sign of the XMCD signal). Furthermore, we see a rich fine structure for V XMCD at the $L_{3,2}$ edges. All this can be nicely interpreted if in parallel the theory calculates the absorption cross section as a function of energy for the XMCD. A full relativistic spin-polarized KKR Greens function method receives perfect agreement with the experiment [19].

In several theories, the so-called integral 'sum rules' were developed in which the areas under the $L_{3,2}$ edges, respectively, are used to separate the orbital and spin moments [20]. This is shown in Fig. 5b. The difference of the area under the L_3 and L_2 signals is related to the spin moment (thin solid line) and the sum of the two areas is proportional to the orbital moment (dotted line). For Fe we clearly see that both yield a positive total area. In conclusion, μ_S and μ_L are parallel aligned. The new results for the V edges show the difficulties to separate the areas of L_3 and L_2, but if we still try to do so, we see that the solid line stays with a negative integral area whereas the dotted line crosses zero; in other words, μ_S^V is antiparallel to Fe whereas μ_L^V is parallel to Fe. This is consistent with a simple atomic picture and the Hund rules. Vanadium, at the beginning of the 3d series, should have as atom an antiparallel alignment. We would like to mention that this is not always the case. In another investigation at the Fe/W interface it was shown that μ_S and μ_L of the induced moment for the W-atoms are parallel aligned, in contrast to what would have been

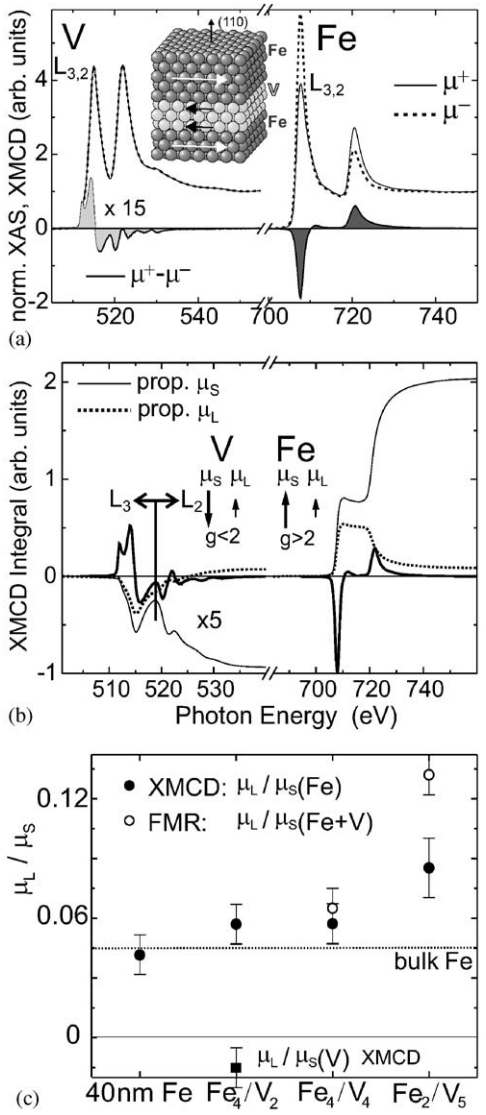

Fig. 5. Fe_5/V_3/Fe trilayer: (a) XAS and XMCD spectra for V and Fe; (b) integrated XMCD spectrum. Orbital and spin moments show different signs for V, but are parallel aligned for Fe; (c) the ratio of μ_L/μ_S measured by FMR [18] and XMCD [19].

expected because W is also located at the beginning of the 5d series [21].

The classical way to separate orbital and spin moments is to measure for example the sum of both in a magnetization measurement (SQUID, etc.) and their ratio μ_L/μ_S. Here, already Kittel has shown that the g factor is a good measure of the ratio $\mu_L/\mu_S = (g-2)/2$. Some results of these experiments are shown in Fig. 5c. On the x-axis, an increasing Fe 'dilution' is shown. For bulk Fe, the g value is given to be $g = 2.09$ corresponding to μ_L/μ_S of 4.5%. We see in Fig. 5c that this ratio increases up to 9–13% for Fe_2/V_5. This schematic diagramm is very interesting because we plot the results of two experimental techniques; FMR (open circles) measures the collective response of Fe + V, whereas XMCD measures element-specific Fe (full circles). For Fe + V, the orbital moment is increased and spin moment is reduced (see Fig. 5b), resulting in a ratio of about 13% (for details see Ref. [19]). In the same way we have added for Fe_4/V_2 the XMCD measurement (full square). There, both moments are antiparallel aligned and consequently the ratio for V is negative (below zero).

All examples given in Sections 2–5 demonstrate a tight collaboration between experiment and theory, leading to a better understanding of magnetism on an atomic scale.

Acknowledgements

This work has been performed in collaboration with E. Kosubek, J. Lindner, A. Scherz, R. Nünthel and H. Wende. Ongoing discussions with the theory groups of K.H. Bennemann, H. Ebert, D.L. Mills, W. Nolting, P. Weinberger and R. Wu are acknowledged. This work was supported in part by DFG, Sfb290 and BMBF (05KS1 KEB4).

References

[1] Z. Zhang, et al., Phys. Rev. Lett. 73 (1994) 336.
[2] A. Layadi, et al., J. Magn. Magn. Mater. 176 (1997) 175.
[3] S.M. Rezende, et al., J. Appl. Phys. 85 (1999) 5892.
[4] D.E. Bürgler, et al., J. Phys.: Condens. Matter 15 (2003) S443.
[5] W. Platow, et al., Phys. Rev. B 59 (1999) 12641.
[6] R. Hammerling, et al., Phys. Rev. B 68 (2003) 092406.
[7] O. Hjortstam, et al., Phys. Rev. B 55 (1995) 15026.
[8] K. Baberschke, in: K. Baberschke, M. Donath, W. Nolting (Eds.), Bandferromagnetism, Lecture Notes in Physics, Vol. 580, Springer, Berlin, 2001, p. 27.
[9] C. Uiberacker, et al., Phys. Rev. Lett. 82 (1999) 1289.
[10] J. Lindner, et al., Phys. Rev. Lett. 88 (2002) 167206.
[11] P. Poulopoulos, et al., J. Phys.: Condens. Matter 15 (2003) S443.
[12] A. Scherz, et al., J. Synchrotron Rad. 8 (2001) 472.
[13] P.J. Jensen, et al., Phys. Rev. B 60 (1999) R14994.
[14] J. Lindner, et al., J. Phys.: Condens. Matter 15 (2003) R193;
J. Lindner, et al., J. Phys.: Condens. Matter 15 (2003) S465.
[15] L. Lindner et al., Phys. Rev. B 68 (2003) 060102(R).
[16] F. Wilhelm, et al., Phys. Rev. Lett. 90 (2003) 129702.
[17] F. Wilhelm, et al., Phys. Rev. Lett. 80 (2000) 314; ESRF Highlights, 2000, p. 63.
[18] A. Anisimov, et al., Phys. Rev. Lett. 82 (1999) 2390.
[19] A. Scherz, et al., Phys. Rev. B 66 (2002) 184401.
[20] H. Ebert, Rep. Prog. Phys. 59 (1995) 1665.
[21] F. Wilhelm, et al., Phys. Rev. Lett. 87 (2001) 207202.